ISSN : 0974 - 7486 Volume 9 Issue 6

Materials Science

Trade Science Inc.

An Indian Journal

Full Paper

MSAIJ, 9(6), 2013 [217-226]

High temperature oxidation behaviour of chromium-rich iron-based alloys containing high carbides fractions

Patrice Berthod*, Moussa Ba, Ahmed Dia
Institut Jean Lamour (UMR 7198), Team 206 "Surface and Interface, Chemical Reactivity of Materials"
University of Lorraine, Faculty of Science and Technologies, B.P. 70239, 54506 Vandoeuvre-lès-Nancy, (FRANCE)
E-mail: patrice.berthod@univ-lorraine.fr

ABSTRACT

Six alloys based on {Fe-30wt.%Cr} and containing from 2.5 to 5.0 wt.%C, were synthesized by foundry way then tested in oxidation at high temperature. The obtained types of microstructures were hypo-eutectic, eutectic or hyper-eutectic, this depending on the carbon content. The alloys were all composed of a metallic Fe(Cr) matrix and of high fractions of carbides (mainly Cr_7C_3). Polished samples were exposed to air during 50h at 1000, 1100 and 1200°C. The oxidized surfaces and affected sub-surfaces were analyzed. The bulk microstructures were also characterized to specify the microstructures at high temperature. The oxides were composed of an outer thick $(Fe,Cr)_2O_3$ scale and of a thin inner layer of Cr_2O_3. In the sub-surface a thin carbide-free zone generally has appeared just under the oxide scale. All alloys seem having correctly resisted against oxidation at 1000 and 1100°C, but the three carbon-richest ones (4 to 5 wt.%C) obviously suffered catastrophic oxidation.

KEYWORDS

Iron alloys;
Chromium;
High carbon content;
High carbide fraction;
High temperature oxidation.

INTRODUCTION

Iron alloys with high carbon content may generally containing large fractions of of hard phases able to lead to high values of hardness for the alloys. In binary Fe-C alloys, pro-eutectic cementite (Fe_3C) and ledeburite (austenite-cementite eutectic) appeared during solidification of white cast irons[1,2] or the {ferrite + Fe_3C} eutectoid compound (pearlite) present in carbon steels[3] are examples of such hard phases or compounds. Other examples are the not-stable phases which can be obtained by quenching steels or SG cast irons from the austenitic domain (martensite)[4]. For more complex alloys, containing other carbides-forming elements, other hard carbides particles can be obtained. For instance, when chromium is present the iron-based alloy are able to reach high levels of hardness thanks to the appearance at solidification of numerous interdendritic chromium carbides, as in some iron-based bulk alloys[5] or of hardfacing coatings[6]. High levels of both carbon and chromium may lead to bulk alloys, which are easy to elaborate by casting and which may display first high volume fractions of carbides for an enhanced hardness and wear resistance. They may also show a good resistance to high temperature oxidation, which can be useful in case of temperature increase due to friction in service. Chromium, which was first added as carbide-former element then plays a second role: forming a protective oxide scale[7]. However, in contrast with superalloys containing the same levels of chromium[8], this element is maybe not so efficient against oxidation in such alloys containing high chromium carbides. Indeed a great part of chromium is trapped in carbides and is maybe not so available to diffuse towards the oxidation front, while the matrix, impoverished in chromium, may be not able to supply chromium with a sufficient flux.

The aim of the present work is to study, at several high temperatures, the oxidation behavior of six ternary iron alloys displaying chromium and carbon contents typical of alloys for wear applications, especially synthesized by conventional casting, with regards to the carbides quantity.

MATERIALS AND METHODOLOGY

Composition of the studied alloys; synthesis

Six compositions {Fe-30wt.%Cr}+ xC with a carbon content x (wt.%) equal to 2.5 (alloy “Fe25”), 3.0 (“Fe30”), 3.5 (“Fe35”), 4.0 (“Fe40”), 4.5 (“Fe45”) and 5.0 (“Ni50”) were chosen for this work. Thermodynamic calculations were first performed to know by anticipation the stable microstructures of the corresponding real alloys at the temperatures of the oxidation tests, as well as the chromium repartition between matrix and the chromium carbides. These calculations were performed by using the Thermo-Calc software[9] and a database which contains the descriptions of the Fe–Cr–C system and of its sub-systems[10-16]. The same software was thereafter also used for obtaining some information about the carbon content in the sub-surface after oxidation.

The six alloys were elaborated by foundry in inert gas (atmosphere of pure argon, 300mbar), by melting pure elements (>99.9%, Alfa Aesar) using a high frequency induction furnace (CELES). Solidification was achieved in the water-cooled copper crucible of the furnace in which the melting occurred. Each obtained ingot (mass of about 40g) was cut into four compact samples of about 125 mm^3. One sample was prepared for the examination of the as-cast microstructure, and the three others were used for the oxidation tests.

Oxidation tests; metallographic characterization

After surface preparation, the samples were exposed to the laboratory air in a resistive tubular furnace for 50 hours, and thereafter cooled outside in ambient air. One sample per alloy was oxidized at 1000°C, the second one at 1100°C and the third one at 1200°C.

The as-cast samples and the oxidized samples were embedded in a cold resin mixture (Araldite CY230 + Strengthener Escil HY956), then cut in two parts (Buehler Isomet 5000 precision saw), then polished under water (SiC papers from 120 to 1200 grit) and finished to obtain a mirror-like state (textile paper containing 1μm–alumina particles). Metallographic observations involved a Scanning Electron Microscope (SEM, XL30 Philips) used essentially in the Back Scattered Electrons mode (BSE) with an acceleration voltage of 20 kV. Additionally, X-Ray Diffraction was performed using a Philips X-Pert Pro diffractometer (wavelength Cu Kα) to specify the phases present in the bulk at the temperatures of the oxidation tests. A Cameca SX100 microprobe (Wavelength Dispersion Spectrometry) was used to obtain WDS profiles over the oxide scales still present on surface and the oxidation-affected sub-surfaces of the alloys, to specify the oxides’ natures and estimate the chromium depletion.

Vickers indentations were performed in the bulk of the oxidized alloys using a Testwell Wolpert apparatus (load: 30kg), to value the possible hardness variation in the bulk during the oxidation tests.

RESULTS AND DISCUSSION

Initial microstructures of the alloys

After solidification and solid-state cooling down to room temperature the six alloys display the microstructures rich in carbides illustrated in Figure 1. These as-cast microstructures allow showing first that the alloys are of the hypo-eutectic type for Fe25, almost eutectic (Fe30) and of the hyper-eutectic type for the four carbon-richest alloys (Fe35 to Fe50). Indeed dendrites of matrix can be seen in the first alloy, even if the main compound is obviously a {matrix + carbides} eutectic. The alloy containing 3.0wt.% of carbon is wholly made of this eutectic compound, and coarse acicular carbides are additionally present in the alloys containing between 3.5 and 5.0wt.% C.

High temperature microstructures according to thermodynamic calculations

Before performing the oxidation tests on these alloys the metallurgical stable states at the oxidation test temperatures were carried out using Thermo-Calc in order to better know the repartition of the two most oxidable elements present in these alloys: Cr and C. The results are presented in three tables.

TABLE 1 : Types and mass fractions of the phases theoretically present in the microstructures of the studied alloys at the temperatures of the oxidation tests (Thermo-Calc calculations).

Phases	1000°C	1100°C	1200°C
Fe25	mat.FCC (58.01%) + $M_{23}C_6$ (41.99%)	mat.FCC (65.50%) + M_7C_3 (8.78%) + $M_{23}C_6$ (25.73%)	mat.FCC (77.09%) + M_7C_3 (22.91%)
Fe30	mat.FCC (68.68%) + M_7C_3 (31.32%)	mat.FCC (70.04%) + M_7C_3 (29.96%)	mat.FCC (71.75%) + M_7C_3 (28.25%)
Fe35	mat.FCC (63.33%) + M_7C_3 (36.67%)	mat.FCC (64.71%) + M_7C_3 (35.29%)	mat.FCC (66.41%) + M_7C_3 (33.59%)
Fe40	mat.FCC (57.97%) + M_7C_3 (42.03%)	mat.FCC (59.34%) + M_7C_3 (40.67%)	mat.FCC (61.01%) + M_7C_3 (38.99%)
Fe45	mat.FCC (52.52%) + M_7C_3 (47.48%)	mat.FCC (53.86%) + M_7C_3 (46.15%)	mat.FCC (55.47%) + M_7C_3 (44.53%)
Fe50	mat.FCC (46.93%) + M_7C_3 (53.07%)	mat.FCC (48.20%) + M_7C_3 (51.80%)	mat.FCC (49.73%) + M_7C_3 (50.27%)

In the first one (TABLE 1) one can see that the matrix ought to be always austenitic since the predicted network is Face Centered Cubic for the six alloys at the three temperatures. The carbides ought to be M_7C_3 in most cases: for the five alloys containing more than 3.0wt.%C and for the one containing 2.5wt.% but at 1200°C only. For the latter one $M_{23}C_6$ carbides are expected at 1000°C and the two types of carbides may co-exist at 1100°C. Thanks to the very high carbon contents of these alloys the carbides are very present in term of mass fractions, even for the C-lowest of these alloys (Fe25) at 1000°C since it contains the low carbon-consuming $M_{23}C_6$ carbides (42% in mass of carbides). Generally the carbide's fraction increases logically when the alloy's carbon content increases (e.g. from 31 to 53% between the Fe30 and Fe50 alloys) and decreases when the temperature increases (a loss of about 3% of carbides in mass between 1000 and 1200°C). Many of these mass fractions may lead to more than 50% in volume fraction thanks to the lower density (less than 7g cm^{-3} at room temperature) of carbides by comparison to matrix (more than 7g cm^{-3}), confirming what one can qualitatively feel by examining some SEM micrographs of Figure 1. Furthermore obtaining more than 50% of carbides in mass fraction is already observed for the Fe50 alloy at the three temperatures. In such alloy the main phase is the carbide phase and no longer the matrix although the latter is the continuous one in the microstructure.

Predicted repartitions of chromium and carbon at high temperature

At the high temperature envisaged for the oxidation tests, chromium and carbon are the two most oxidable elements, as this can be confirmed by consulting Ellingham diagrams. It is then of importance to know how these two elements are distributed in the microstructures, especially since chromium (useful for keeping a good behavior on long times by forming a protective scale of chromia on the alloys) and carbon (which oxidizes in gaseous species able to perturb this external chromia scale) may be more or less mobile if there are trapped in the carbides or in solid solution in the matrix. Thermodynamic calculations may be of great usefulness to estimate the compositions of the matrix (for the too light element carbon) and of the carbides (for both Cr and C because of the small size of some of these particles).

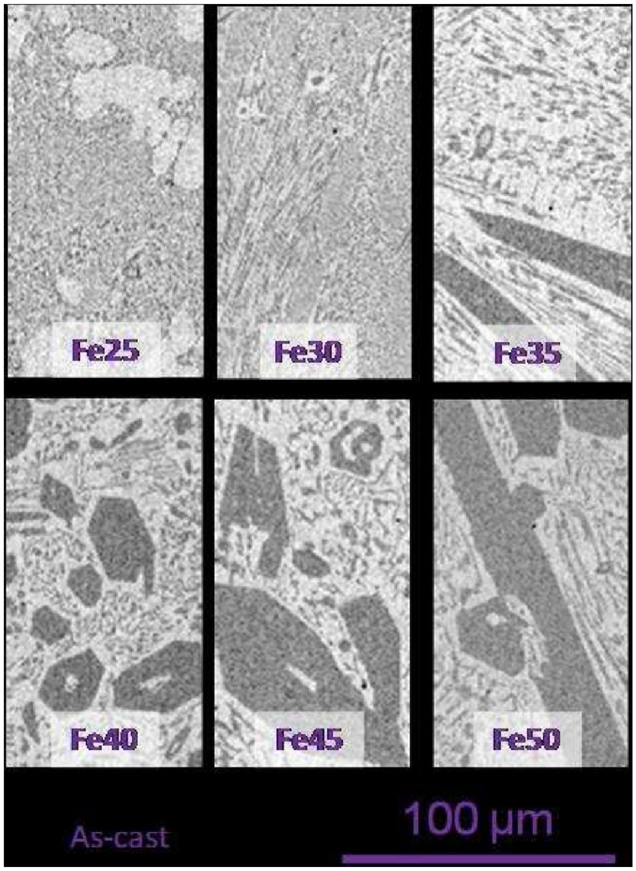

Figure 1 : As-cast microstructures of the six alloys issued from foundry practice (SEM micrographs taken in BSE mode).

The theoretical compositions of the FCC matrix at 1000, 1100 and 1200°C are given in TABLE 2. One can first note that the contents in chromium and in carbon obey the same trends versus temperature (they both increases when the considered temperature increase, consequences of the decrease in carbide mass fraction at constant stoichiometry). In contrast they follow opposite ways when the alloy's carbon content increases at constant temperature: the chromium content decreases and the carbon content increases:

- Concerning chromium the content decreases from about 18 to 9wt.% at 1200°C between Fe25 and Fe50, and from only 12 to a little more than 5wt.% at 1000°C. Such low chromium contents, especially for the C-richest alloys, may be not sufficient to allow a chromia-forming behavior if only matrix can participate to the chromium supplying of the oxidation front.
- Concerning carbon its content may reach more than 1 wt.%C in the matrix (Fe50 at 1200°C), as is to say about four times this value in atomic percent ! However this remains lower than the 2wt.% of maximal solubility of carbon in austenite in the case of binary Fe-C alloys (at the eutectic temperature of about 1150°C). Such high contents of carbon present in solid solution in matrix, as is to say in conditions of high mobility (notably for such small atoms), are likely to favour intense emission of CO_x gases with the disturbing effect attended against the protective scales.

TABLE 2 : Chromium and carbon weight contents in the matrix at the temperatures of the oxidation tests (Thermo-Calc calculations).

wt.%Cr in matrix wt.%C in matrix	1000°C		1100°C		1200°C	
Fe25	11.81	0.31	14.67	0.45	18.07	0.60
Fe30	11.48	0.32	13.55	0.49	15.59	0.69
Fe35	9.18	0.40	11.32	0.59	13.44	0.80
Fe40	7.47	0.50	9.55	0.70	11.66	0.93
Fe45	6.23	0.62	8.18	0.83	10.21	1.06
Fe50	5.33	0.74	7.13	0.96	9.04	1.20

The theoretical weight contents in chromium and in carbon issued from thermodynamic calculations for the six alloys and the three temperatures are given in TABLE 3. The chromium content in the M_7C_3 carbides tends to decrease when the carbon content increases. More carbon logically leads to a higher participation of iron, element more present in the alloys than chromium which is fixed to 30wt.%). The slow carbon weight content evolution is only due to this Fe/Cr ratio variation, since the atomic weight of Fe and Cr are not the same (52g Mol^{-1} for Cr and 56g Mol^{-1} for Fe). Carbides may thus act as an important supplier of chromium to feed the oxidation front if their dissolution is sufficiently fast, but unfortunately they may also release high quantities of carbon and consequently of carbon oxide gases, with the possible detrimental effect on a protective oxides scales.

TABLE 3 : Chromium and carbon weight contents in the carbides at the temperatures of the oxidation tests (Thermo-Calc calculations); The difference to 100% of the sum is the Fe content in the carbide phases.

wt.%Cr in carbides wt.%C in carbides	1000°C		1100°C		1200°C	
Fe25	55.13*	5.53*	**		70.12	8.88
Fe30	70.60	8.88	68.47	8.87	66.60	8.86
Fe35	65.95	8.85	64.26	8.84	62.73	8.83
Fe40	61.07	8.82	59.84	8.81	58.69	8.81
Fe45	56.30	8.79	55.46	8.79	54.65	8.78
Fe50	51.82	8.76	51.28	8.76	50.74	8.76

For all alloys and all temperatures the carbide phase is $(Cr,Fe)_7C_3$ (*except for: *Fe25 at 1000°C for which the carbide is $(Cr, Fe)_{23}C_6$ and ** Fe25 at 1100°C in which carbides are both $M_{23}C_6$ (55.32%Cr, 39.15%Fe, 5.53%C) and M_7C_3 (70.19%Cr, 20.93%Fe, 8.88%C).

General surface and sub-surface states of the oxidized samples

Three samples per alloy were exposed to high temperature oxidation in laboratory air for 50 hours at 1000°C, 1100°C or 1200°C. After cooling (in air out of furnace), the embedded and polished oxidized samples were examined by electron microscopy, which led to the micrographs presented in Figure 2 for the Fe25 to Fe35 alloys and in Figure 3 for the Fe40 to Fe50 alloys. Qualitatively it appears generally that most of the samples correctly resisted high temperature oxidation, except the three carbon-richest ones at 1200°C (Figure 2). Indeed very thick oxides have obviously grown on the Fe40, Fe45 and Fe50 when they were exposed at 1200°C, by consuming the alloys from their external surface and by replacing them by more than 1mm of multi-constituted oxides. Furthermore oxidation at 1200°C seem having had other consequences for these alloys especially rich in carbon and initially in carbides: they are now absent over a deep zone from the {thick oxide – alloy} interface (several hundredths µm) and the ones still existing in the samples core seems having known a decrease in surface fraction. In contrast the other samples oxidized at only 1100 or 1000°C and the three carbon-lowest alloys oxidized at each of the three temperatures display not so thick oxides on their surfaces and not so deep carbides-free zones.

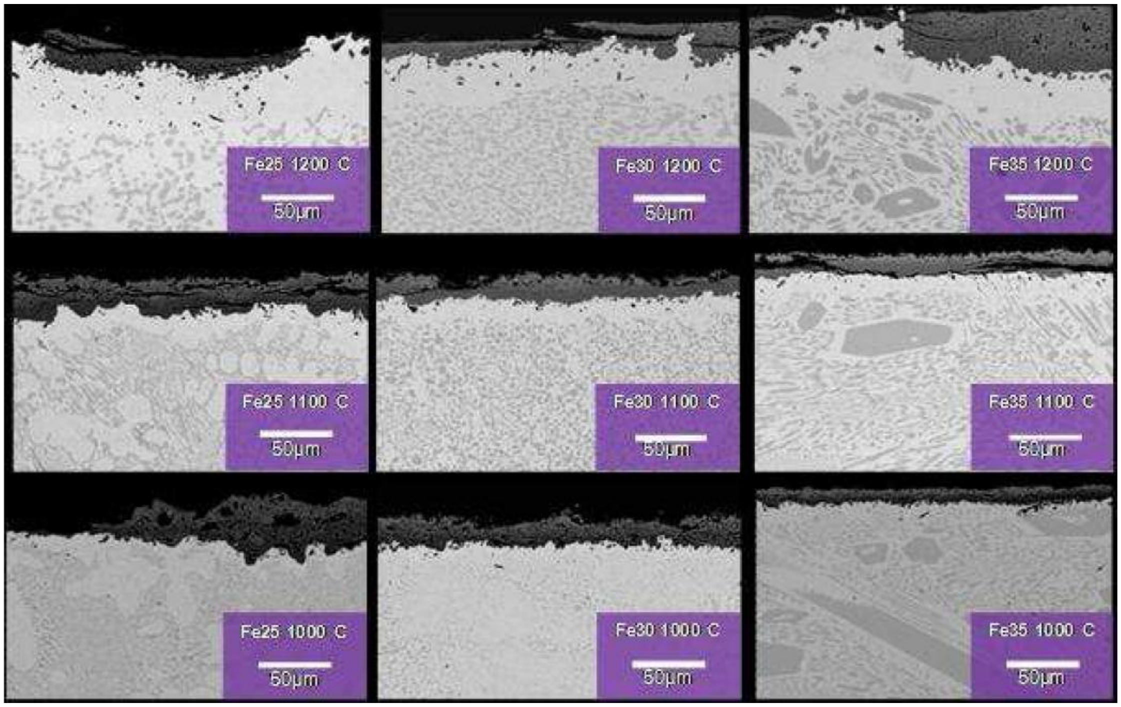

Figure 2 : Surface states of the three carbon-lowest alloys after 50 hours of oxidation at the three temperatures (SEM micrographs taken in BSE mode).

Characterization of the external oxides

As it can be seen on the micrographs presented in Figure 2 and Figure 3, the oxide scales remaining on the surface of the samples appear irregular, fissured or broken. The cooling obviously induced the loss of parts of these oxides formed at high temperature, under the usual stresses due to their difference of thermal contraction with the substrate. This oxide spallation was probably favored by the multi-oxide structures of these scales as well as their bad compactness due to high levels of porosity. It was then not tried to measure their average thickness. However the natures of these oxides were specified by performing WDS concentration profiles. As often encountered for chromium-rich iron-based alloys, and as this may be suspected from the different levels of gray seen in the scales on the SEM/BSE micrographs of Figure 2 and Figure 3 (inner layer much darker than the outer layer), the oxides formed over the studied alloys are multiple. When chromia is present, this is as an inner layer existing between the alloy and other oxides (Figure 4). Furthermore chromia can be purely Cr_2O_3 in some cases (e.g. Figure 4 left) but it generally also contains iron, either in small quantities (e.g. Figure 4 right) or with levels similar to the chromium ones (e.g. Figure 5). In that latter case one often sees that the chromium content in the $(Fe,Cr)_2O_3$ decreases from the inner part to the outer part of this oxide, the iron content displaying the inverse trend (e.g. Figure 5 left). The carbon-richest alloys present some areas where oxidation was particularly fast (notably at 1100 and 1200°C), leading to very thick oxides. In addition to the preceding oxides, these thick scales are addition alloy composed of a most external part of Fe_2O_3 (e.g. Figure 6), the presence of which clearly shows that the concerned alloys have totally lost the chromia-forming behavior that they still demonstrated for lower temperatures.

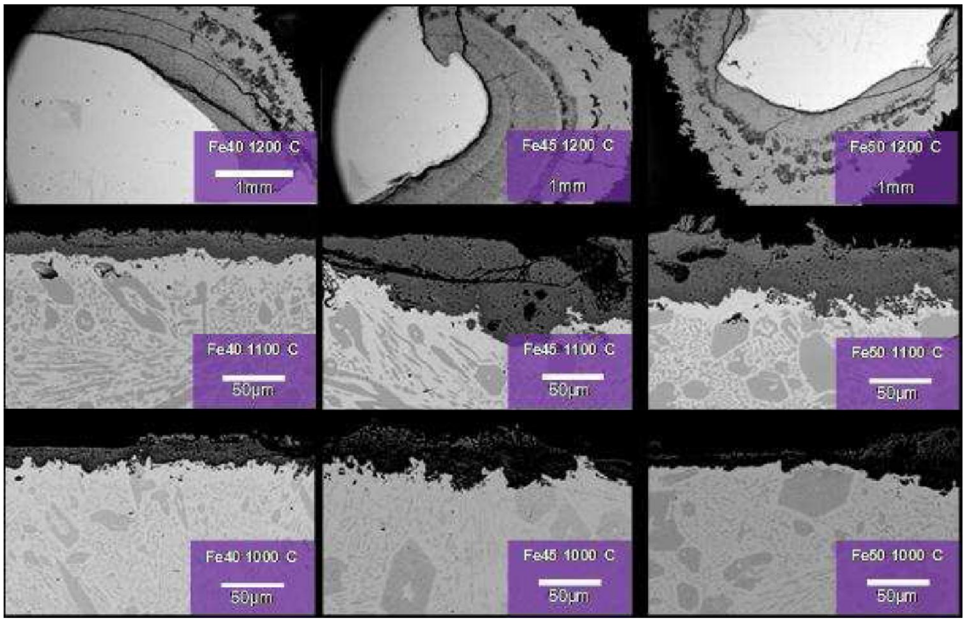

Figure 3 : Surface states of the three carbon-richest alloys after 50 hours of oxidation at the three temperatures (SEM micrographs taken in BSE mode).

Characterization of the sub-surfaces

These natures of oxides may be put in relation with the chromium contents in the alloys on extreme surface. The minimal values measured on the WDS profiles are displayed in TABLE 4. These values are still rather high for the three carbon-lowest alloys (for which they tend to increase with temperature) but they are significantly lower for the three carbon-richest alloys since many of these surface chromium contents are close to 10wt.% and even lower in some cases. When these values (TABLE 4) are compared with the Cr-contents predicted in the matrix by Thermo-Calc for the same temperatures (TABLE 2) it appears that these minimal chromium contents measured on extreme surface are almost equal to the matrix ones, and often more or less higher the latter ones. A little deeper the chromium contents are higher again, this being a consequence of the actual dissolution of carbides which seem to playing their role of reservoirs of chromium that they release to feed the oxidation front by diffusion through the carbide-free zone previously formed.

These carbide-free zones were measured and the average values of their depths are given in TABLE 5. It appears that, at a given temperature, the carbide-free zone developed slower for alloys richer in carbides (except Fe40, Fe45 and Fe50 at 1200°C) but faster for a given alloy for a higher temperature. This remains true until the formed oxide is still protective: when oxidation becomes catastrophic (Fe40, Fe45 and Fe50 at 1200°C) carbides disappear rapidly over much deeper areas from the external surface, revealing a fast consumption of both chromium and carbon.

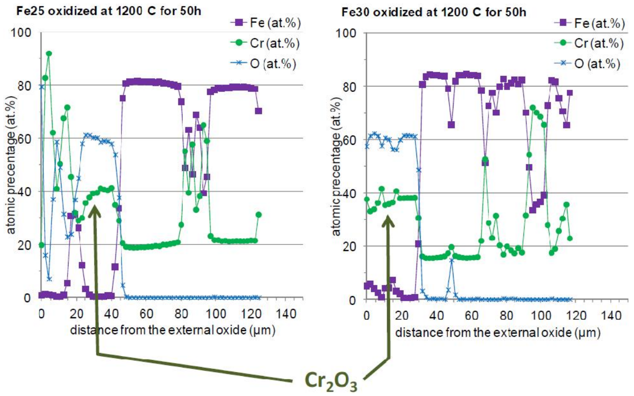

Figure 4 : WDS microprobe profiles revealing the presence of chromia either as an inner layer separating the alloy from more complex oxides (left) or as a single oxide (right).

This disappearance of carbides due to oxidation led to decide verifying if the natures of the bulk's carbides, the surface fraction of which seem unchanged between before and after oxidation tests (maybe except after exposure to 1200°C: little decrease in surface fraction), were or not affected by oxidation. Experiments of X-Ray Diffraction were carried out, leading to spectra, some examples of which being displayed in Figure 7 and Figure 8. It appears that the high temperature natures of the carbides were kept ($Cr_{23}C_6$ and/or M_7C_3 in Fe25 and M_7C_3 in the other alloys), after the post-oxidation cooling which was not too slow to allow the possible medium and low temperature carbides changes. In contrast the FCC matrix was generally partly transformed into its BCC low temperature type.

TABLE 4 : Minimal chromium weight contents near the external surface (one WDS profile per oxidized alloy).

wt.%Cr on surface	1000°C	1100°C	1200°C
Fe25	17.2	15.2	18.0
Fe30	11.2	15.4	14.8
Fe35	11.6	12.3	15.5
Fe40	18.3	11	/
Fe45	6.0	8.3	/
Fe50	8.3	15.4	/

TABLE 5 : Average depths of the carbide-free zone.

Carbide-free zone depth (µm)	1000°C	1100°C	1200°C
Fe25	7	14	45
Fe30	6	12	34
Fe35	7.6	12	34
Fe40	7.6	12	610
Fe45	3.5	5.9	500
Fe50	0	4.7	640

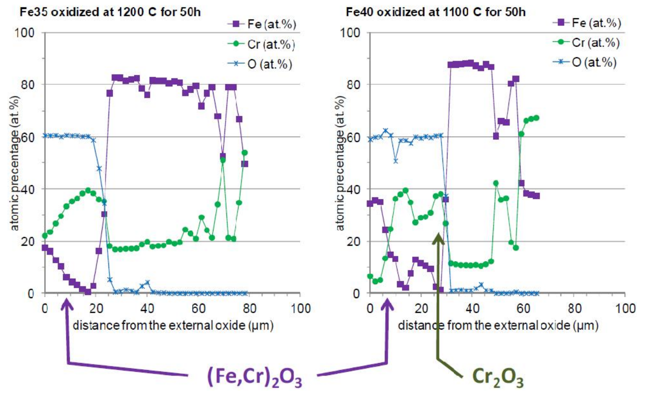

Figure 5 : WDS microprobe profiles revealing the presence of tri-oxide of chromium and iron simultaneously, separated from the alloy with a more or less thick chromia sub-layer; illustration (left) of the increase in {Fe/Cr} ratio by moving {int. → ext.} through the $(Fe,Cr)_2O_3$ oxide.

General commentaries

Despite their very high contents in carbon the studied alloys present microstructures which are all double-phased {matrix + carbide}, except Fe25 when stabilized at 1100°C, which contains also the FCC matrix and simultaneously two types of carbides. In contrast as encountered in Nickel-based alloys[17] and Cobalt-based alloys[18] graphite never appeared, neither in the as-cast microstructures nor in the ones stabilized at 1000, 1100 and 1200°C. Thus, at high temperature, a great part of chromium is involved in the formation in the numerous carbides especially as these ones (M_7C_3) are not the chromium-richest ones (the Cr-richest $M_{23}C_6$ are present only in the Fe25 alloy at the two lowest temperatures of interest here). Fortunately these carbides also contain a part of iron instead chromium, and in addition, there is a significant part of carbon atoms which are not involved in carbides but stay in solid solution in the matrix at high temperature (e.g. more than 1wt.% out of the 5wt.%C of the Fe50 alloy, according to Thermo-Calc calculations). However this leads to a matrix strongly impoverished in this element which is of great importance for the resistance against high temperature oxidation. The most characteristic case is the great difference between the 30wt.%Cr in the whole Fe50 alloy and the 5.3wt.%Cr in its matrix at 1000°C, according to Thermo-Calc calculations.

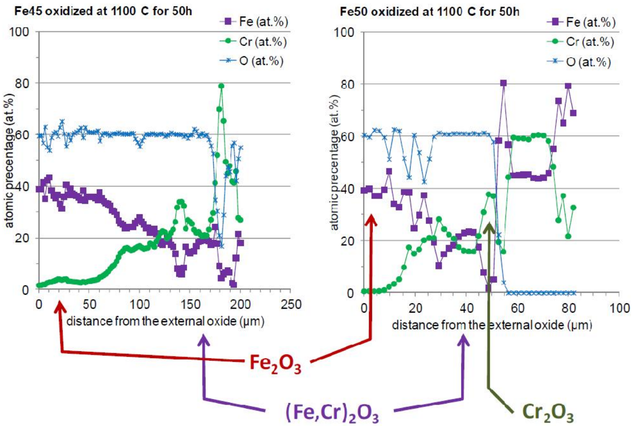

Figure 6 : WDS microprobe profiles illustrating the {Fe_2O_3 → $(Fe,Cr)_2O_3$ → Cr_2O_3} succession by crossing the whole oxide thickness from the air/oxide interface towards the oxide/alloy interface, in the case of the two carbon-richest alloys where they were severely oxidized.

Fortunately it appeared that the chromium contained in the carbides can be generally released thanks to the carbide's dissolution in order to rise and maintain at a higher level the chromium content in the sub-surface matrix, more precisely in the newly appeared carbide-free zone. One can logically think that the carbon in solid solution in the matrix close to the oxidation front diffused rapidly and left the samples as gaseous oxi-

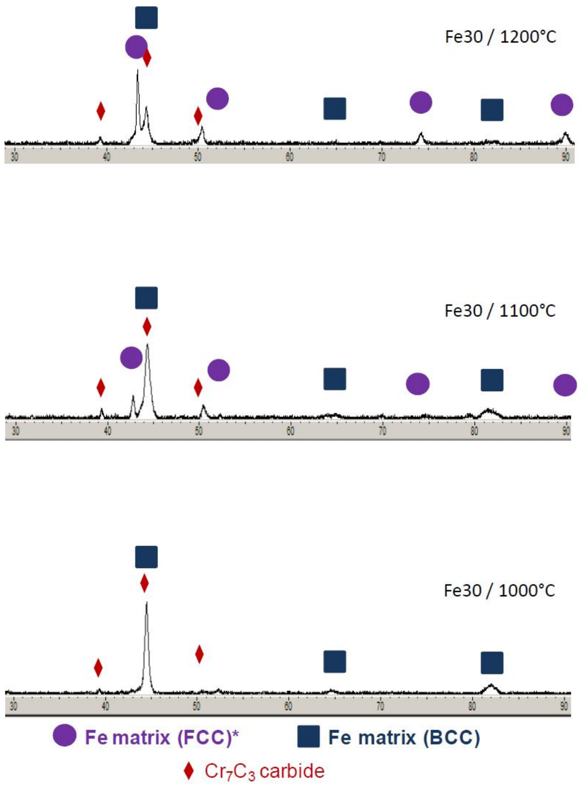

Figure 7 : XRD spectra acquired in the bulk of the Fe30 alloy after oxidation at 1000, 1100 or 1200°C.

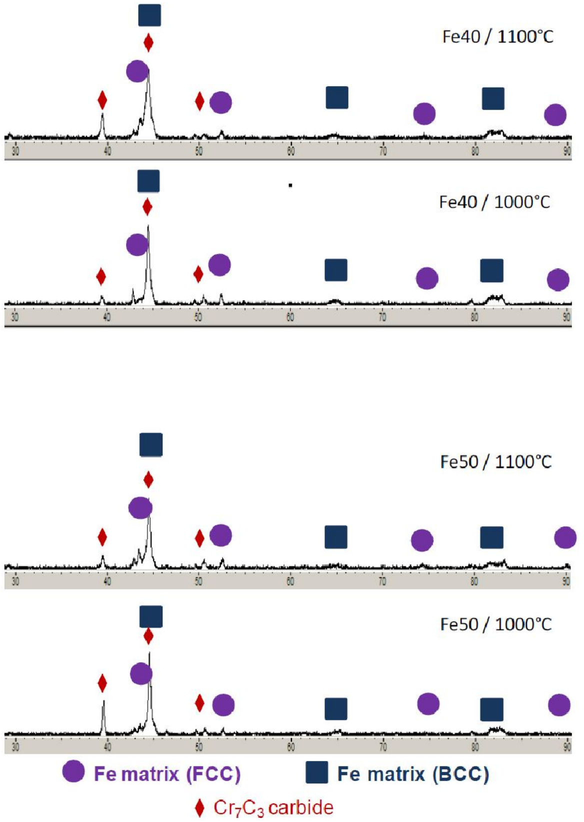

Figure 8 : XRD spectra acquired in the bulk of the Fe40 and Fe50 alloys after oxidation at 1000 or 1100°C.

dized species, with consequently a destabilization of the neighbor carbides which become dissociated in carbon and chromium atoms. This allowed supplying these areas in new chromium atoms which diffuse towards the oxidation front. It appeared in most cases that the kinetic of carbide's dissolution and of the resulting chromium releasing was high enough to maintain, not a chromia-forming behavior but rather a $(Fe,Cr)_2O_3$-forming behaviour. The presence of $(Fe,Cr)_2O_3$ external scales, eventually separated from the metallic substrate with a thinner sub-layer of Cr_2O_3, is usual after oxidation at high temperatures for chromium-rich iron-based alloys with not so high carbon contents, and the high temperature oxidation behavior of the studied carbon-rich alloys is not much worse than for the low C iron alloys with the same Cr content[19,20], except of course the three C-richest alloys notably at 1200°C.

Nevertheless one can think that these alloys especially rich in carbon are more threatened by the imminence of general oxidation than C-lower similar alloys since their chromium contents on extreme surface are significantly lower than the latter ones, as shown in Figure 9 in which the surface Cr contents after the 50 hours of oxidation at the three temperatures are graphically presented together with similar previous results obtained for C-lower 30wt.%Cr-containing ternary iron alloys. It can be also noticed that, although the external scales formed are of the same nature (i.e. mainly $(Fe,Cr)_2O_3$), these oxides are here much more porous than for the C-lower alloys. This difference may be due to the carbon content especially high in the alloys studied here, for which one can imagine the releasing of higher volumes of gaseous carbon oxides during oxidation. The worse quality resulting for these external scales is of course detrimental for their protective role. In addition the low Cr contents of extreme surface may result from a dissolution of the carbides which is not fast enough. The competition of kinetics between the chromium consumption at the oxidation front and the chromium releasing by dissolving carbides seems becoming unfavorable since the depth of the carbide-free zone after 50 hours of oxidation continuously decreases when the carbon content in alloy increases, as already seen above (TABLE 5) but as more generally evidenced in Figure 10 in which older results concerning C-lower 30Cr-containing iron alloys are added: especially deep for the alloys with 0 to 0.8wt.%C, the carbide-free depth falls to a low level for the alloy with 1.2wt.%C and goes on decreasing until reaching almost 0 µm for the Fe50 alloy after oxidation at 1000 and 1100°C. The kinetic competition has become too difficult for the dissolution of the carbides of the Fe40, Fe45 and Fe50 alloys, the carbides of which were especially coarse for many of them, which did not allow them to help the oxidation resistance of their matrix particularly poor in chromium (around 10wt.% and even lower).

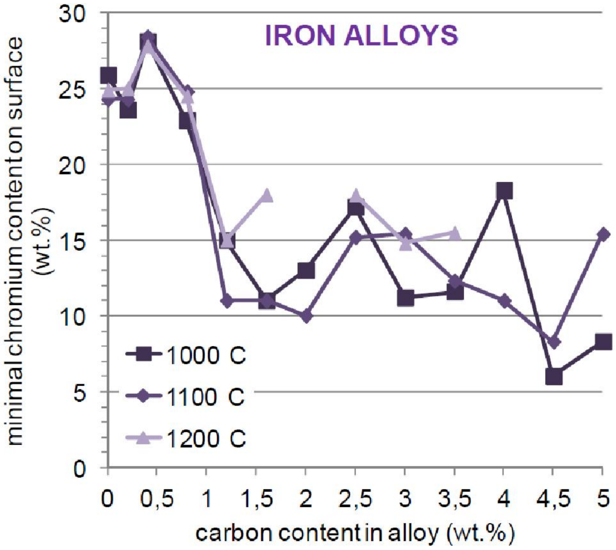

Figure 9 : Evolution, versus the alloy's carbon content and the oxidation temperature, of the chromium content on the extreme surface of the oxidized alloys (at theoxide/alloy interface).

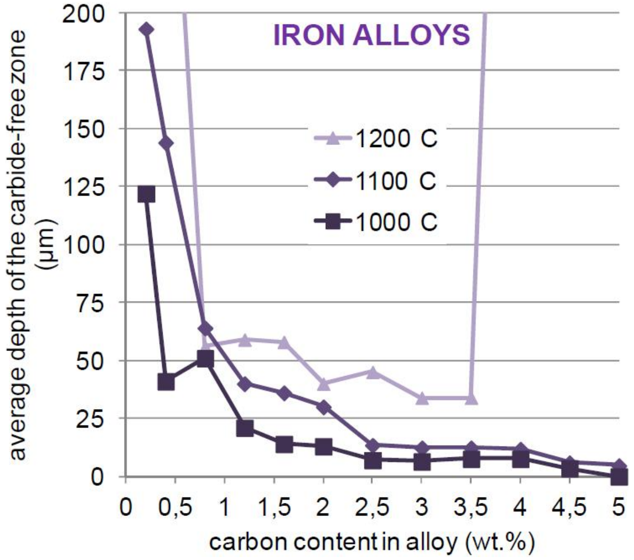

Figure 10 : Evolution of the average depth of the carbide-free zone versus the alloy's carbon content and the oxidation temperature.

Catastrophic oxidation effectively occurred before 50 hours in three cases: Fe40, Fe45 and Fe50 at 1200°C. The corresponding samples were being consumed all around, with the fast growing of multi-constituted non-protective oxides, with even a thick external part of hematite (Fe_2O_3) covering the $(Fe,Cr)_2O_3$ oxide, a very deep carbide-free zone under the oxidation front, and a progressing desappearance of carbides in the bulk.

These phenomena lead not only to a decrease in size of the still metallic part of these samples but also to a fall of its hardness (Figure 11). It can be noticed that the other samples were also affected by at least little modification of their carbides (especially after exposure to 1200°C), as metallographically observed and as revealed by a lower but significant softening in Figure 11 too. This softening is obviously more pronounced for the alloys studied here than for the Fe-30Cr-2.0C alloy earlier studied after exposures at the same temperatures[21], the hardness values of which are added in Figure 11 for comparison. In contrast, the hardness of the six alloys have seemingly increased by comparison with the ones measured in the as-cast conditions. This may result from the presence of a part of matrix which is still compact FCC after cooling, harder than the less compact BCC (Back Centered Cubic) one, as shown by the XRD measurements.

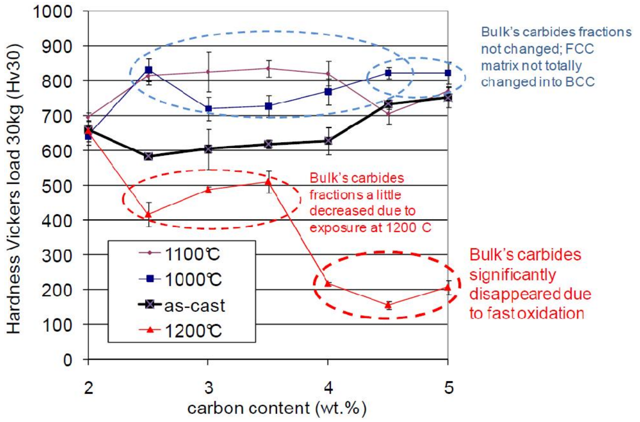

Figure 11 : Evolution of the average hardness versus the alloy's carbon content and the oxidation temperature.

To finish one can remark that it was not really possible to try correlating the thickness of oxides (measured where they were not lost by spallation) and the chromium quantities having left the alloys. Indeed the oxides were first not only of chromium but also of both

Fe and Cr with variable parts of each metallic element, and second the interface oxide/alloy did not stay at the same position but obviously moved inwards, as suggested by the irregular interface and by the participation of iron in significant quantities in the external oxides. For the same latter reason it was not envisaged to value the carbon lost by the alloy, and then the volume of gaseous carbon oxides formed to explain further the amount of porosities in the oxides.

CONCLUSION

The six studied alloys demonstrated behaviors in high temperature oxidation which were rather good with respect to their especially high levels of carbon and volume fractions of carbides and the low chromium content resulting in the matrix. Carbides effectively assume the role of chromium reservoir for allowing the alloys resisting high temperature oxidation, in addition to the high hardness and the wear resistance that these hard particles bring to this type of alloy. However there may exist a limit of service temperature, identified as 1200°C for 50°C in air for a 30wt.%Cr-containing alloy with more than 4wt.%C, for which an inadequacy appears between the consumption rate of chromium and the kinetic of chromium releasing by dissolution of the carbides. Further work can be envisaged to shift farer this limit, for example by choosing higher chromium contents for enriching matrix in this element at constant carbide's fractions, or by improving the fineness of the coarse primary carbides using either faster cooling rate or inoculants.

ACKNOWLEDGEMENTS

The authors wish to thank Olivier Rouer for the WDS measurements, Pascal Villeger for the X-Ray diffraction runs and Th. Schweitzer for his technical help.

REFERENCES

[1] G.Lesoult; Solidification: Cristallisation et microstructures. Techniques de l'ingénieur, Paris, **(1986)**.
[2] W.Kurz, D.J.Fisher; Fundamentals of solidification, Trans.Tech.Publ., Switzerland, **(1989)**.
[3] M.Durand-Charre; Microstructure of steels & cast irons, Springer, **(2004)**.
[4] A.Litwinchuck, F.X.Kayser, H.H.Baker, A.Henkin; Journal of Materials Science, **11(7)**, 1200 **(1976)**.
[5] H.E.N.Stone; Journal of Materials Science, **14(12)**, 2781 **(1979)**.
[6] B.V.Cockeram; Metallurgical and materials transactions A, Physical Metallurgy and Materials Science, **33(11)**, 3403 **(2002)**.
[7] D.J.Young; High temperature oxidation and corrosion of metals, Elsevier, Amsterdam, **(2008)**.
[8] M.J.Donachie, S.J.Donachie; Superalloys: A technical guide, 2nd Edition, ASM International, Materials Park, **(2002)**.
[9] N.Thermo-Calc Version; http://www.thermocalc.com, Foundation for computational thermodynamics Stockholm, Sweden, Copyright, **(1993, 2000)**.
[10] A.Fernandez Guillermet, P.Gustafson; High Temperatures - High Pressures, **16(6)**, 591 **(1984)**.
[11] J.O.Andersson; International Journal of Thermophysics, **6(4)**, 411 **(1985)**.
[12] P.Gustafson; Carbon, **24(2)**, 169 **(1986)**.
[13] J.O.Andersson, B.Sundman; Calphad, **11(1)**, 83 **(1987)**.
[14] P.Gustafson; Scandinavian Journal of Metallurgy, **14(5)**, 259 **(1985)**.
[15] J.O.Andersson; Calphad, **11(3)**, 271 **(1987)**.
[16] J.O.Andersson; Metallurgical Transactions A, **19(3)**, 627 **(1988)**.
[17] P.Berthod, E.Souaillat, O.Hestin, P.Lemoine, T.Schweitzer; Annales de Chimie – Science des Matériaux, **35(5)**, 291 **(2011)**.
[18] P.Berthod, O.Hestin, E.Souaillat, P.Lemoine, G.Michel, L.Aranda; Annales de Chimie – Science des Matériaux, **36(3)**, 193 **(2011)**.
[19] P.Berthod; Annales de Chimie – Science des Matériaux, **33(3)**, 247 **(2008)**.
[20] P.Berthod, P.Lemoine, L.Aranda; Materials Science Forum, **595-598**, 871 **(2008)**.
[21] P.Berthod; Materials Science and Technology, **25(8)**, 1003 **(2009)**.